The influence of pickup protons, from interstellar neutral hydrogen, on the propagation of interplanetary shocks from the Halloween 2003 solar events to ACE and Ulysses: A 3-D MHD modeling study

T. R. Detman,[1] D. S. Intriligator,[1] M. Dryer,[1,2] W. Sun,[1,3] C. S. Deehr,[1,3] and J. Intriligator[1,4]

Received 16 June 2010; revised 8 November 2010; accepted 23 November 2010; published 23 March 2011.

[1] We describe our 3-D, time-dependent, MHD solar wind model that we recently modified to include the physics of pickup protons from interstellar neutral hydrogen. The model has a time-dependent lower boundary condition, at 0.1 AU, that is driven by source surface map files through an empirical interface module. We describe the empirical interface and its parameter tuning to maximize model agreement with background (quiet) solar wind observations at ACE. We then give results of a simulation study of the famous Halloween 2003 series of solar events. We began with shock inputs from the Fearless Forecast real-time shock arrival prediction study, and then we iteratively adjusted input shock speeds to obtain agreement between observed and simulated shock arrival times at ACE. We then extended the model grid to 5.5 AU and compared those simulation results with Ulysses observations at 5.2 AU. Next we undertook the more difficult tuning of shock speeds and locations to get matching shock arrival times at both ACE and Ulysses. Then we ran this last case again with neutral hydrogen density set to zero, to identify the effect of pickup ions. We show that the speed of interplanetary shocks propagating from the Sun to Ulysses is reduced by the effects of pickup protons. We plan to make further improvements to the model as we continue our benchmarking process to 10 AU, comparing our results with Cassini observations, and eventually on to 100 AU, comparing our results with Voyager 1 and 2 observations.

Citation: Detman, T. R., D. S. Intriligator, M. Dryer, W. Sun, C. S. Deehr, and J. Intriligator (2011), The influence of pickup protons, from interstellar neutral hydrogen, on the propagation of interplanetary shocks from the Halloween 2003 solar events to ACE and Ulysses: A 3-D MHD modeling study, *J. Geophys. Res.*, *116*, A03105, doi:10.1029/2010JA015803.

1. Introduction

[2] Data beamed back to Earth by the Voyager 1 and 2 spacecraft from the fringe of our heliosphere offer us an opportunity to test and improve our understanding of this dynamic and complex region near the outskirts of our neighborhood in space.

[3] The spherically expanding solar wind comes into pressure balance with the local interstellar medium (LISM) through the termination shock (TS) which greatly reduces the solar wind speed. Pressure fluctuations in the turbulent solar wind make the location of the termination shock highly dynamic; it moved across Voyager 2 five times [*Richardson et al.*, 2008; *Burlaga et al.*, 2008; *Intriligator et al.*, 2010a, 2010b]. Pressure variations resulting directly from solar activity include interplanetary shock waves, coronal mass ejections (CMEs), corotating interaction regions (CIRs), and global merged interaction regions (GMIRs). While both Voyager spacecraft were still inside the TS, they both observed very large pressure variations associated with the Halloween 2003 series of solar events.

[4] The LISM contains neutral hydrogen atoms that drift unperturbed through the heliosheath and TS into the heliosphere. As this neutral hydrogen approaches the Sun, it begins to ionize by charge exchange with solar wind protons and through photoionization. These pickup protons transfer momentum and energy into the solar wind. Due to their high relative velocities, they slow and heat the solar wind. Heavier neutral atoms are also present in the LISM and become pickup ions, but we will not discuss them here.

[5] Our broad goal is to validate this new model, consistent with its simplicity. That is, to benchmark our progress in understanding and modeling the solar wind and the propagation of solar disturbances to the outer heliosphere. And, our specific goal is to study the evolution of the

[1]Carmel Research Center, Santa Monica, California, USA.
[2]Space Weather Prediction Center, NOAA, Boulder, Colorado, USA.
[3]Geophysical Institute, University of Alaska Fairbanks, Fairbanks, Alaska, USA.
[4]Bangor University, Bangor, UK.

0148-0227/11/2010JA015803

Halloween 2003 storm chain disturbances as they propagate to the ACE, Ulysses, Cassini, Voyager 1, and 2 spacecraft. An important aspect for both goals is the influence of pickup protons on the solar wind flow, and on shock propagation. Toward these goals, we have added the basic physics of pickup protons (as mentioned above) to the Hybrid Heliospheric Modeling System (HHMS) [*Detman et al.*, 2006], a time-dependent three-dimensional (3-D) magnetohydrodynamic (MHD) solar wind model. The purpose of this paper is to describe the modified model, HHMS-PI, and to describe our initial results in simulating the propagation of the Halloween 2003 solar events to ACE and Ulysses. We expect to continue improving the model as we progress outward.

[6] An important and distinguishing feature of our model is that it has a dynamic time-dependent lower boundary condition close to the Sun (0.1 AU) that is driven through an empirical interface by solar photospheric, coronal, X-ray, and radio observations.

[7] We take a step-by-step approach, beginning with the tuning of empirical model parameters to make the model agree with the background solar wind at ACE. Then we move to the Halloween 2003 solar events, and introduce shock input perturbations. We iteratively adjust the shock inputs, first to match ACE observations, then we extend the grid and compare model results with Ulysses observations, near 5 AU. Next we use both ACE and Ulysses observations to further constrain shock inputs. We describe the results of that exercise, and show comparisons with Ulysses solar wind observations. The comparisons with the SWICS pickup proton density measurements at Ulysses and our model results are described in work by D. Intriligator et al. (Initial benchmarking of pickup proton modeling and Ulysses SWICS measurements: Comparisons with the three-dimensional MHD HHMS-PI simulation, submitted to *Journal of Geophysical Research*, 2010).

[8] We focus on the asymmetrical, 3-D, and time-dependent nature of the heliosphere, and we stress verification at each step, using quantitative comparisons of simulation results with spacecraft observations. Next we plan to use ACE, Ulysses, and Cassini observations to further constrain shock inputs, then extend the grid to 100 AU, and use those results to better understand Voyager 1 and Voyager 2 observations. Both Voyagers were still inside the TS when the Halloween 2003 shocks reached them, although the precise associations between the Halloween 2003 solar events and the arrival times of specific shocks in the plasma and field data from V2 and V1 have yet to be determined. We think, that by continuing to improve our model, and by using observations from ACE, Ulysses and Cassini to constrain shock inputs, that we can contribute toward determining those associations. We must also note that we would not necessarily expect our model runs to contain a TS, even though the locations where the TS was later observed by the Voyagers would be within the model grid. One reason is that we currently use a simple zero- to first-order extrapolation scheme to set our outer grid boundary condition, thus the model does not "feel" the full LISM pressure. We believe simulated conditions immediately upstream of the TS would be useful. Simulated conditions beyond the observed location of the TS, although incorrect, should still have some correlation with actual conditions.

[9] During the Halloween 2003 superstorm, three active regions (ARs) produced 124 soft X-ray flares, and more than 60 coronal mass ejections (CMEs) between 18 October and 5 November. Two CMEs hit Earth head-on resulting in huge geomagnetic storms. A review of the solar and terrestrial events was provided by *Veselovsky et al.* [2004]. A first set of predicted shock arrivals at Earth from some of these events was made as part of the Fearless Forecast [*Dryer et al.*, 2004]; we refer to it again later.

[10] Although they were not based on a full 3-D MHD treatment, these earlier efforts to model the shock propagation did yield promising results. Because of the relative nearness of the Earth to the Sun, some of the specific nonlinearities and other effects that can only be accurately modeled in a full 3-D treatment did not overly influence the predictions. However, when modeling shock propagation to further distances, these effects can become large and thus must be included in a proper model. Furthermore, it should be emphasized that the unique orbits and positions of the various spacecraft and the spatially and temporally varying solar flares, CMEs, and high-speed streams necessitate full 3-D treatment. Finally, accurate and self-consistent input conditions at, or close to, the Sun are essential.

[11] This methodology, which includes accurate background and shock input descriptions along with full 3-D treatment, has been emphasized (as mentioned earlier) in exploratory work of *Intriligator et al.* [2005a, 2005b, 2005c, 2006, 2007, 2008], who initiated this 3-D MHD approach with the Hybrid Heliospheric Modeling System (HHMS) out to 5 AU without the inclusion of pickup protons. They also employed a computationally nonintensive "quick-look" 3-D kinematic model (Hakamada-Akasofu-Fry: HAFv.2). This latter model has also been used for real time space weather objectives [*Fry et al.*, 2001, 2003; *Dryer et al.*, 2004; *McKenna-Lawlor et al.*, 2006; *Smith et al.*, 2009b, 2009a].

[12] Section 2 will discuss the extension of HHMS to HHMS-PI to include consideration of pickup protons. Section 3 will lay out the sequence of simulation, verification, model, and shock input tuning steps performed. Section 4 gives results, and section 5 will contain discussion and concluding remarks.

2. The Model

[13] The Hybrid Heliospheric Modeling System (HHMS) began with an apparently simple idea for improving solar wind forecasts at Earth with a few days' lead time [*Detman et al.*, 2006]. A number of papers had already demonstrated predictive ability for solar wind at Earth using source surface models [*Wang and Sheeley*, 1988, 1990; *Wang et al.*, 1996, 1997; *Fry et al.*, 2001; *Zhao and Hoeksema*, 1993, 1994, 1995; *Detman and Vassiliadis*, 1997]. More recent results with source surface models are described by *Arge and Pizzo* [2000] and *MacNiece* [2009]. Yet these models are based on relatively simple physics (potential field extrapolation, via Laplace's equation) from the photosphere through the solar corona to a specified "source surface" where an outer boundary condition of a purely radial magnetic field is applied. Source surface height is typically around $2.5R_S$, where R_S is the mean solar radius, 695000 km. The average Sun-Earth distance is about $215R_S$, so these models typically

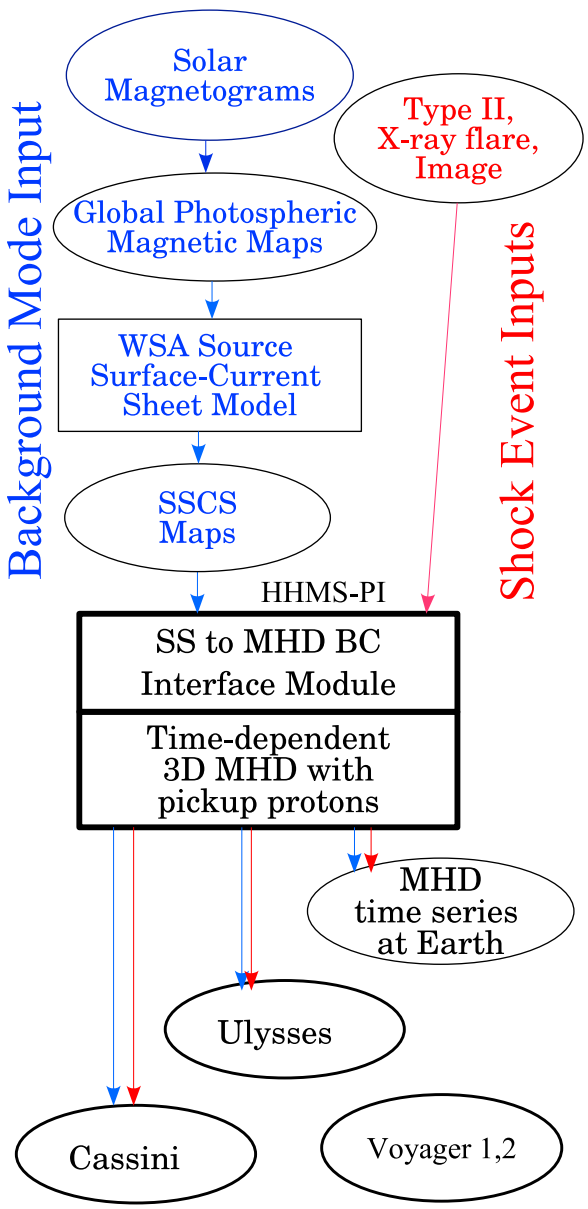

Figure 1. HHMS-PI block diagram.

covered less than 1.2% of that distance. The simple idea was that, by extrapolating a source surface solution only to 0.1 AU, it could be used to specify the lower boundary conditions of an MHD solar wind model (such as the present one and others), which would then cover the remaining 90% of the distance to Earth.

[14] A block diagram of HHMS-PI is shown in Figure 1. Note there are two independent paths by which solar observations drive the MHD boundary conditions.

[15] The background mode begins with solar magnetograms, top left in the block diagram. Daily magnetograms, over a solar rotation, about 27 days, are combined to make a global photospheric magnetic map. These photospheric maps provide the lower boundary condition for the WSA Source Surface Current Sheet model [*Arge and Pizzo*, 2000], which in turn gives a global solution for the magnetic field from the photosphere to the source surface. The HHMS-PI interface module generates time-dependent MHD boundary conditions for the solar wind model by interpolating between two SSCS maps separated in time by a solar rotation or less. This input path generates the slowly changing "background" solar wind. A more detailed discussion of the interface module is given later.

[16] The solar event input mode starts on the top right side of the block diagram in Figure 1. This input path applies an impulsive perturbation to the existing background boundary conditions in order to simulate the explosive release of energy in solar flares and CMEs. The intent of this input path is to introduce shock waves into the model grid, based on observed characteristics of type II radio sweeps and locations of solar flares and CMEs. The shock event inputs are start time, duration, latitude, longitude, perturbation radius (angle subtended from the center of the Sun), and shock speed. The preexisting boundary conditions are modified according to the Rankine-Hugoniot relations for the specified shock speed.

[17] The interface module does four things: (1) it translates from source surface map parameters to solar wind MHD parameters; (2) it extrapolates from source surface height to MHD boundary height ($21.5Rs = 0.1AU$); (3) it introduces the effect of solar rotation; and (4) it introduces time dependence by interpolating in time between two source surface map files. The HHMS-PI interface module reads source surface maps in Flexible Image Transport System (FITS) format as generated and archived in near real time by NOAA's Space Weather Prediction Center at http://www.swpc.noaa.gov/ws/. These maps are generated by the Wang-Sheeley-Arge Source Surface Current Sheet (SSCS) model [*Arge and Pizzo*, 2000] which is a potential field model with an added current sheet; in this model the source surface height is $2.5R_S$, but with the current sheet, the solution is given at $5R_S$. These SSCS map files contain global maps, at $5R_S$ and 5° × 5° angular resolution, of various parameters; we make use of the following three: radial magnetic field on the source surface, *ssBr*; flux tube expansion factor, *ssEf*; and foot point distance, on the photosphere, to the closest coronal hole boundary, *ssFd*. For efficiency in development and testing the HHMS-PI also has angular resolution of 5° × 5° to match the SSCS map files. In the radial direction the grid resolution is $1.76R_S$. We plan to improve grid resolution in future work.

[18] Pickup protons are insignificant at 0.1 AU, but for numerical reasons they cannot be set to zero or left uninitialized. Thus, they are initialized and held at very small values until the source terms in their conservation equations become significant. This occurs beyond 0.5 AU, for the small values we used in equations (9) and (10).

[19] HHMS-PI operates in Solar Equatorial spherical coordinates (r, θ, ϕ), and has ten MHD variables, as follows: three components of velocity (U_r, U_θ, U_ϕ), three components of magnetic field (B_r, B_θ, B_ϕ), and two densities and two pressures for solar wind and pickup protons, (Ds, Dp) and (Ps, Pp), respectively. The model grid covers 360° in longitude (the ϕ direction) with a periodic boundary condition; it goes from +57.5° to −57.5° in latitude (the θ direction), and 0.1 to 5.5 AU in radius. The computational MHD equations for these ten variables, in conservation form, are given in Appendix A. Note, by solving the MHD

Table 1. Original Fearless Forecast Shock Descriptions[a]

FF Event Number	Date of the Flare	Time at Beginning of Flare	LAT (deg)	LON (deg)	VS (km/s)	TAU	VSW (km/s)	XMAX	XEND	OPT	XRAY
507	19 Oct 2003	1650	N05	E56	625	120	575	1650	1704	NA	X1.1
508	21 Oct 2003	0347	S10	E90	1058	40	740	0345	0406	SF	C7.8
509	22 Oct 2003	0938	S02	E22	650	300	575	0956	0959	NA	M1.7
510	23 Oct 2003	0827	S21	E88	967	130	500	0835	0849	1B	X5.4
511	25 Oct 2003	0415	S15	E43	316	200	550	0417	0528	2N	M1.2
512	26 Oct 2003	0617	S18	E44	1500	300	460	0654	0733	3N	X1.2
513	26 Oct 2003	1735	N05	W38	1700	330	460	1819	1921	2N	X1.2
514	28 Oct 2003	1102	S16	E08	3200	300	800	1110	1124	NA	X17.2
515	29 Oct 2003	2044	S15	W02	2700	130	650	2049	2101	2B	X10.0
516	1 Nov 2003	2234	S12	W60	400	100	575	2238	2249	1N	M3.3
517	2 Nov 2003	1714	S14	W56	2000	100	525	1725	1739	2B	X8.3
518	3 Nov 2003	0124	N10	W83	1600	145	500	0130	0145	2B	X2.7
519	3 Nov 2003	0956	N08	W77	1100	130	520	0955	1019	2F	X3.9
520	4 Nov 2003	1943	S19	W83	2380	130	630	1929	2006	3B	X40
521	11 Nov 2003	1335	S03	W61	492	300	750	1351	1417	SF	M1.6
522	13 Nov 2003	0924	N01	E90	1100	300	650	0929	1002	NA	M1.4
523	17 Nov 2003	0917	S01	E33	1100	200	NA	NA	NA	1N	M4.2
524	18 Nov 2003	0747	N00	E18	950	300	NA	NA	NA	2N	M3.2
525	20 Nov 2003	0747	N01	W08	900	45	NA	NA	NA	2B	M9.6

[a]FF, Fearless Forecast event number; LAT, flare heliolatitude with respect to disk center; LON, flare heliolongitude with respect to disk center; VS, estimated shock speed; TAU, shock driving time duration in HHMM format (hours, minutes); VSW, background solar wind speed; XMAX, time of maximum X-ray flux; XEND, time of X-ray flare end; OPT, optical classification; XRAY, NOAA X-ray classification; NA, no data available. See *Dryer et al.* [2004] for details.

equations in conservation form, the model is able to capture shocks.

[20] The MHD solar wind model in HHMS-PI operates under the assumption of hyperbolic boundary conditions. This means the flow speed on the grid boundary must be faster than any characteristic wave speed in the plasma. Specifically, this means, $U_r > F_S$, where F_S is the fast mode wave speed and $F_S^2 = C_S^2 + V_A^2$, where C_S is the sound speed, and V_A is the Alfvén speed; $C_S^2 = \gamma Ps/Ds$, and $V_A^2 = B_r^2/(\mu Ds)$. Two difficulties are encountered in designing the interface. One difficulty is that the interface model has to mimic the main plasma physics of the corona that is missing from all source surface models, and that is computationally intensive for MHD models. The second difficulty is that our original choice of 0.1 AU for the lower grid boundary has turned out to be too close to the Sun (closer than the Alfvén critical point) a little too often. The first problem is fundamental. Our approach to solve it has been to develop a set of empirical formulas, containing adjustable parameters, for converting three SS map parameters into eight MHD parameters. Due in part to its empirical character, our interface module keeps evolving as we continue to learn and test (benchmark) new approaches. We will say more about this in section 4. The second problem is not fundamental; we can simply raise the lower grid boundary. This would reduce, but not eliminate, the occurrence of solar wind conditions when the Alfvén critical point is within the grid. This would also increase the volume of space that this simple empirical model must account for.

[21] The empirical translation from three source surface parameters to eight MHD boundary condition parameters currently contains five free "tuning" parameters that we tune (optimize) for agreement of the model output with spacecraft observations during quiet (background) solar wind conditions. This could be viewed as a five dimensional nonlinear optimization problem, but, by using observable flow invariants such as r^2B_r, and r^2DsU_r it effectively reduces to a three dimensional search; also the optimum turns out to be smooth and broad. This allows us to find an adequate near-optimum tuning with a reasonable number of model runs.

[22] The choice of a function to maximize, by tuning, is also important. In tuning for agreement with ACE solar wind observations, we used the mean of five skill scores for five different solar wind quantities: speed, U_r; number density, Ns; mass flux, $FM = DsU_r$; and $(B_r - B_\phi)$. Note, $(B_r - B_\phi)$ is the projection of the field onto the Parker spiral; we use it as a measure of interplanetary magnetic field (IMF) polarity. Skill score, also known as prediction efficiency, is defined as 1.0 minus the ratio of mean squared error (MSE) to the sample variance (VAR):

$$skill = PE = 1 - MSE/VAR,$$

where $MSE = \frac{1}{N}\sum_{i=1}^{N}(f_i - x_i)^2$ and $VAR = \frac{1}{N}\sum_{i=1}^{N}(\bar{x} - x_i)^2$.

[23] Perfect, and only perfect, predictions give a skill score, or $PE = 1.0$. This is in contrast to other, often quoted, measures such as the correlation coefficient. (A set of predictions can have a correlation coefficient of 1.0 with the corresponding set of observations, but still have large errors. This makes the correlation coefficient inappropriate for model tuning, and of limited value for verification in general.) However, because the correlation coefficient is a commonly used and familiar parameter, we show both the skill and correlation coefficients on our plots. The correlation coefficient is given by

$$rc = \frac{\sum(f_i - \bar{f})(x_i - \bar{x})}{\left[\sum(f_i - \bar{f})^2 \sum(x_i - \bar{x})^2\right]^{1/2}}.$$

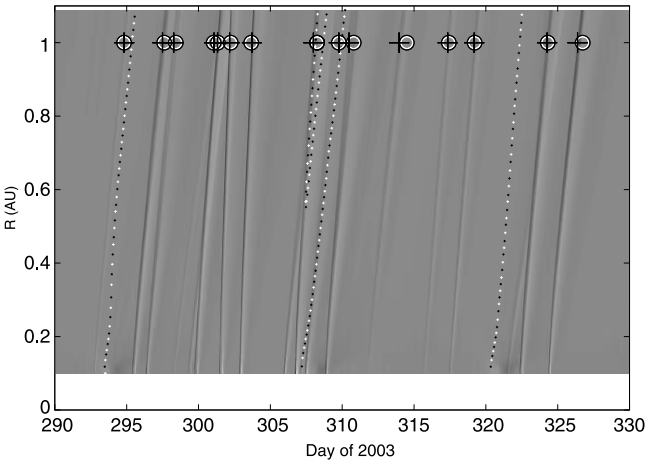

Figure 2. Sun-Earth line r-t plot of shock index. Circles mark observed shock arrivals; plus signs mark simulated shock arrivals. Dotted lines mark magnetic sector boundaries.

A high correlation coefficient between f and x means that a good prediction of x can be made by a *linear transformation* of f.

[24] For the results presented here, our interface module used the following formulas to translate and extrapolate from SS map parameters at 5 Rs to HHMS-PI MHD parameters at 21.5 Rs (0.1 AU):

$$U_r = \mathbf{Vmin} + \mathbf{delV}/ssEf^{\mathbf{Vexp}} + 7.4\left(ssFd/ssEf^{\mathbf{Vexp}/2} - 3.5\right), \tag{1}$$

$$U_\theta = 0, \tag{2}$$

$$U_\phi = \Omega R_\phi \sin\theta, \tag{3}$$

$$B_r = B_{SPEC} ssBr/B_{median}, \tag{4}$$

$$B_\theta = 0, \tag{5}$$

$$B_\phi = V_\phi B_r/U_r, \tag{6}$$

where $V_\phi = U_\phi - \Omega r \sin\theta$,

$$Ds = (B_{SPEC}\mathbf{M_A}/U_r)^2/\mu_0, \tag{7}$$

$$Ps = (Ds/\gamma)(U_r/\mathbf{M_S})^2, \tag{8}$$

$$Dp = 10^{-20}, \tag{9}$$

$$Pp = 10^{-14}. \tag{10}$$

[25] The five empirical tuning parameters, printed in bold in equations (1)–(9), are *Vmin*, *delV*, *Vexp*, M_S, and M_A. Here M_S and M_A specify the sonic and Alfvén Mach numbers, respectively, on the lower grid boundary. Other constants include Ω, the solar rotation rate; R_ϕ, a length scale which determines the azimuthal velocity, U_ϕ, one component of the angular momentum transferred into the solar wind; B_{SPEC}, a fixed strength for the magnitude of the radial magnetic field; here B_{median} is the median of $|ssBr|$ for an individual SS map; and γ is the polytropic index for solar wind protons. As explained by *Detman et al.* [2006], the source surface field, *ssBr*, fluctuates from map to map. In our interface module these fluctuations must be removed to prevent introduction of magnetic monopoles into the model grid. Equation (4) does this by replacing the fluctuating

Table 2. Shock Inputs Adjusted to Match ACE Observed Shock Arrivals[a]

FF Event Number	DOY	VS.g	TAU (h)	LAT	LON	TOAAO	TTO (h)	TOAAS	TTS (h)	VS.h
507	292.701	608	1.33	5	−56	294.819	50.832	294.704	48.07	575.0
508	294.158	517	0.67	−10	−90					517.0
509	295.401	808	3.00	−2	−22	297.604	52.872	297.551	51.60	792.9
510	296.352	904	1.50	−21	−88	299.772	82.080			904.0
511	298.177	526	2.00	−15	−43	300.650	59.352			626.0
512	299.262	921	3.00	−18	−44	301.397	51.240	301.193	46.34	833.0
513	299.733	507	3.50	5	38					507.0
514	301.460	2121	3.00	−16	−8	302.246	18.864	302.212	18.05	2039.6
515	302.864	1720	1.50	−15	2	303.759	21.480	303.692	19.87	1720.0
516	305.940	688	1.00	−12	60					688.0
517	306.718	1570	1.00	−14	56	308.249	36.744	308.197	35.50	1516.7
518	307.058	718	1.75	10	83					718.0
519	307.414	673	1.50	8	77	310.805	81.384			700.0
520	308.822	600	1.50	−19	83	312.518	88.704			600.0
521	315.566	671	3.00	−3	61	317.421	44.520	317.415	44.38	668.8
522	317.392	828	3.00	1	−90	319.214	43.728	319.130	41.71	789.8
523	321.387	547	2.00	−1	−33					547.0
524	322.324	935	3.00	0	−18	324.307	47.592	324.289	47.16	921.4
525	324.324	967	0.75	1	8	326.487	51.912	326.442	50.83	965.2

[a]FF, Fearless Forecast event number, as in Table 1; DOY, day of year with fraction translated from Table 1, second and third columns; VS.g, adjusted shock speed on iteration "g"; TAU, shock driving time duration in hours with fraction; LAT, flare heliolatitude (same as in Table 1); LON, flare heliolongitude; TOAAO, time of shock ACE arrival observed (blank means no observed shock at ACE could be paired with this solar event); TTO, shock travel time observed ((column 7 − column 2) × 24); TOAAS, time of shock ACE arrival simulated; TTS, shock travel time simulated; VS.h, new adjusted shock speed for iteration "g" (VS.h = TTS/TTO × VS.g, as explained in text).

B_{median} with the specified constant B_{SPEC}. For our simulation of the Halloween 2003 events, we used the first 200 days of 2003 for background mode tuning, and we arrived at the following parameter values:

$$\begin{aligned} Vmin &= 154 \quad \text{(km/s)}, \\ delV &= 300 \quad \text{(km/s)}, \\ Vexp &= 0.3, \\ M_S &= 1.28, \\ M_A &= 1.00. \end{aligned}$$

[26] We set the polytropic index, $\gamma = 1.5$ based on work by *Totten et al.* [1996]. We use $B_{SPEC} = 500nT$; this value gives average field strengths at Earth that are usually slightly weaker than observed, however it allows us to keep the Alfvén Mach number tuning parameter, $M_A \geq 1.00$, consistent with our assumption of hyperbolic boundary conditions.

[27] As a starting point we adopted the stationary, spherically symmetrical neutral hydrogen distribution of *Wang et al.* [2000], see Appendix A. In future work, we plan to implement a more realistic neutral hydrogen model that has uniform speed, direction, upstream density, and includes conservation of mass for the neutral hydrogen within the model grid. This might be accomplished with a relatively simple model for the neutral hydrogen, however the HHMS-PI model will then need to be modified to operate in Solar Ecliptic (inertial) coordinates.

3. The Method

[28] Our approach is incremental. We created the HHMS-PI code by modifying its predecessor, HHMS, to solve the equations of ideal MHD solar wind with pickup protons, as described in Appendix A. Next, we used the first 200 days of 2003 for background mode tuning.

[29] Next we introduced the Halloween 2003 series of solar events. We started with the shock strengths, locations, times, and durations given in Table 1. In Table 1, the first seven columns are the Fearless Forecast (FF) event number, the date, time, heliolatitude, heliolongitude, shock speed, and duration given in hhmm format. (The remaining five columns are not used by HHMS-PI.) These parameters were originally posted to an e-mail list in near real time, following solar events, as the Fearless Forecast [*Dryer et al.*, 2004]. These values were used in HHMS-PI to apply shock perturbations directly to the background mode boundary conditions. We simulated the interval from day 285 of 2003 through the end of the year. After applying the shock perturbations, we again compared HHMS-PI results with ACE observation for this time period. Not surprisingly, the agreements between simulated and observed shock arrivals at ACE were less than perfect. In fact, inspection of time series alone was not sufficient to deduce many of the associations between input shock perturbations and simulated (or observed) shock arrivals at ACE.

[30] To make this association, we made radius-time (r-t) plots of an especially designed shock index, $d/dr \log(r^4 \rho F_S)$, along the Sun-Earth line, where $\rho = Ds + Dp$ is total mass density, and, F_S is the fast mode wave speed, $F_S^2 = \gamma P_T/\rho + B^2/(\mu_0\rho)$, where $P_T = P_S + P_P$ is the total thermal pressure. Figure 2 shows such an r-t plot along the Sun-Earth line from a model run of the Halloween 2003 events. With the associations in hand, we then used the simulated time series at ACE, to "zoom in" and get more accurate simulated shock arrival times at ACE.

[31] We then used the ratios of simulated to observed shock travel times to adjust the shock speed inputs in an iterative tuning process. For an isolated shock event this adjustment process usually converges in three or four iterations to make the simulated shock arrival time closely match the observed. For the rapid fire solar events of Halloween 2003, pairing FF events at the Sun with observed shocks at ACE is challenging; shock interactions complicated both the tuning and matching processes. We consider our current pairings, shown in Table 2, to be preliminary. Table 2 shows one iteration (*g* to *h*) of the shock speed adjustment process. In Table 2, date and time have been converted to fractional day of year; TOAAO is time of arrival, ACE, observed; TTO is travel time, observed, in hours; TTS is travel time simulated; and VS.h is the new adjusted shock speed, VS.h = VS.g · TTS/TTO. Figure 3 shows the resulting time series comparisons of HHMS-PI with ACE for the Halloween 2003 interval.

[32] Next, we extended the model grid to 5.5 AU, keeping the neutral hydrogen density at ∞, $N_\infty = 0.1$ cm^{-3}, repeated the last run (that is, we use the ACE tuned shock inputs), and compared model results with observations at Ulysses. Again, this first comparison was not impressive. In order to obtain good comparisons at both ACE and Ulysses, we undertook a somewhat trial and error shock bituning exercise; adjusting mainly the heliolongitude (LON), disturbance radius (RAD), and shock speed (VSH). Table 3 gives the results of that exercise. Figure 4 is an r-t plot, like Figure 2, but showing shocks' propagation along the Sun-Ulysses line, and Figure 5 compares the HHMS-PI simulated time series with Ulysses solar wind observations at 5.25 AU and 103 degrees west of Earth in heliolongitude.

[33] Finally, we repeated this last run with the neutral hydrogen density set to zero in order to isolate the effect of pickup protons on shock propagation. The results of that exercise are shown in Table 4, as promised by the title of this paper. (At ACE, we found no differences in simulated shock arrival times.) In Table 4, $DNH_0 = N_\infty m_p$ is the mass density of neutral hydrogen at infinity (see Appendix A), and DIFF is the delay in shock arrival, in days, due to pickup ions. Our results, in Table 4, show unambiguously that solar-generated interplanetary shock wave speeds are reduced by the presence of pickup protons from the LISM neutral hydrogen flowing into the heliosphere.

4. Discussion

[34] A notable aspect of the shock input bituning (to match shock arrivals at both ACE and Ulysses) is that we could not reproduce the high solar wind speeds seen at Ulysses around day 320 using only the original Fearless Forecast events. Meanwhile, *de Koning et al.* [2005] indicated the occurrence of an unusually fast CME originating from beyond the visible disk of the Sun on 7 November at 1554 UT. On the basis of that information, we added the event listed as FF 520.2 in the first column of Table 3. A longitude of W120, and latitude of S18 is consistent with this event coming from the same active region (NOAA/

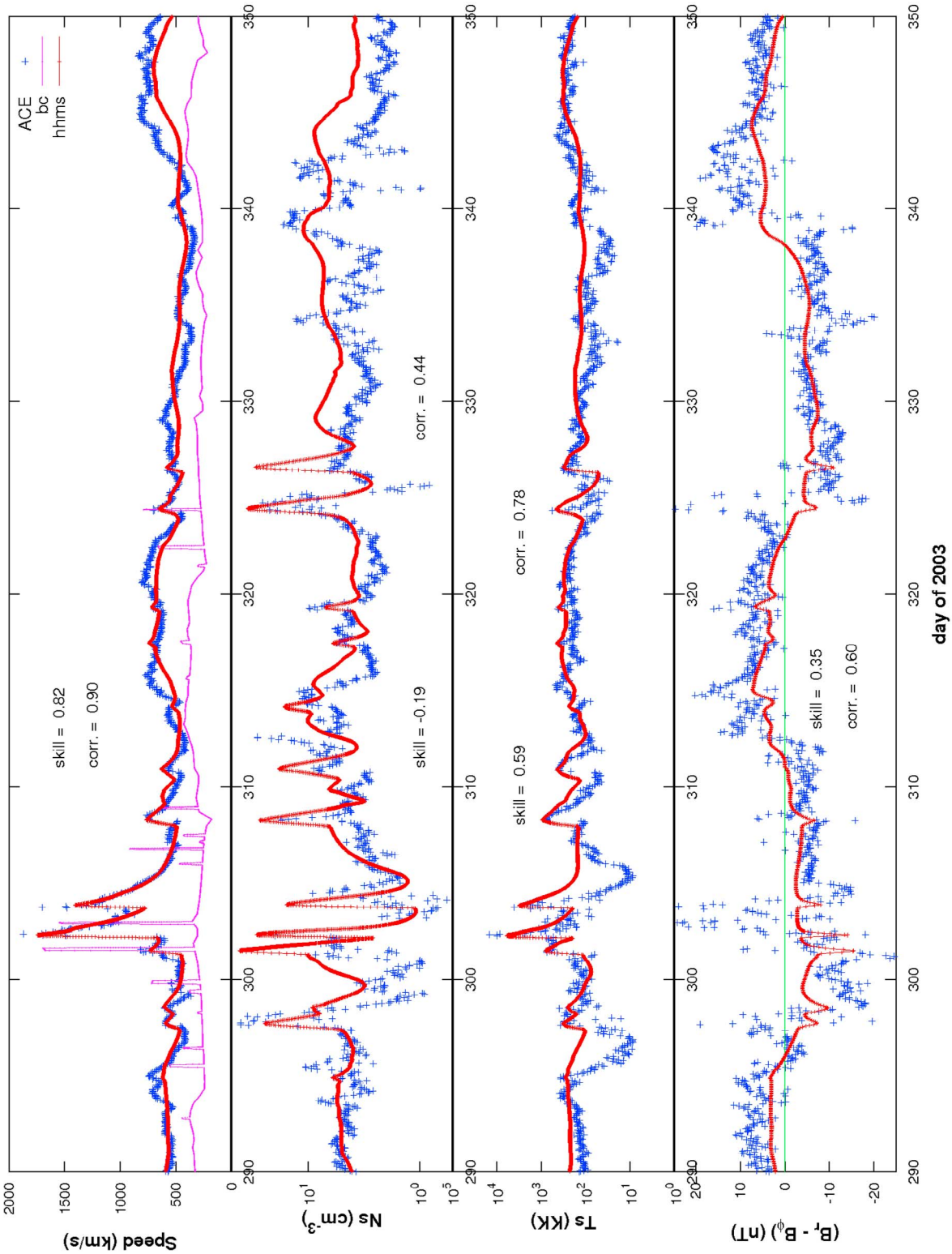

Figure 3. Comparison of HHMS-PI simulated time series at Earth with ACE solar wind observations for the Halloween 2003 study interval. Blue is ACE data. Red is HHMS-PI. Magenta (top only) is the HHMS-PI boundary condition at the sub-Earth point.

Table 3. Shock Inputs Adjusted to Match Both ACE and Ulysses[a]

Event Date	Event Time	DOY	LAT (deg)	LON (deg)	RAD (deg)	VSH (km/s)	TAU (h)	FF
19 Oct 2003	1650	292.701	5	−56	102	519.6	1.3	507
21 Oct 2003	0347	294.158	−10	−90	100	517.0	0.7	508
22 Oct 2003	0938	295.401	−2	−22	100	781.5	3	509
23 Oct 2003	0827	296.352	−21	−88	108	1276.0	1.5	510
25 Oct 2003	0415	298.177	−15	−43	120	530.0	2	511
26 Oct 2003	0617	299.262	−18	−43	120	574.1	3	512
26 Oct 2003	1735	299.733	5	32.6	70.2	1027.0	3.5	513
28 Oct 2003	1102	301.460	−16	−8	120	1951.0	3	514
29 Oct 2003	2044	302.864	−14	1	123	1612.4	1.5	515
1 Nov 2003	2234	305.940	−10	61	120	820.9	1	516
2 Nov 2003	1714	306.718	−14	82.53	158	1791.4	1	517
3 Nov 2003	0124	307.058	10	85	100	725.0	1.8	518
3 Nov 2003	0956	307.414	8	77	120	1131.3	1.5	519
4 Nov 2003	1943	308.822	−19	78.84	102	1580.7	1.5	520
7 Nov 2003	1554	311.663	−18	120	100	1682.7	2	520
11 Nov 2003	1335	315.566	−3	88.77	93.7	807.0	3	521
13 Nov 2003	0924	317.392	1	−90	101	718.5	3	522
17 Nov 2003	0917	321.387	−1	−33	100	547.0	2	523
18 Nov 2003	0747	322.324	0	−18	221.1	918.4	3	524
20 Nov 2003	0747	324.324	1	14	104.9	997.9	0.8	525

[a]DOY, date and time translated to day of year 2003 with fraction; LAT, shock input heliolatitude; LON, shock input heliolongitude; RAD, shock input radius; VSH, shock input speed; TAU, shock input duration; FF, event sequence number.

SWPC AR 10486) that produced FF520, FF517, and/or FF514. When we added this event to our shock inputs and adjusted the shock speed to make the simulated shock arrive at day 318.984, we got a significantly better match to Ulysses velocities around that time, but we also got a greatly improved match with a reverse shock at Ulysses near day 320, that produced the highest speeds at Ulysses in the study interval.

[35] Even in its simplest form that ignores practically all microphysics, ideal MHD can often produce useful global-scale results simply because it conserves mass, momentum, and energy. On the other hand, it is possible to modify or extend the equations of ideal MHD to include specific effects that arise from a more detailed consideration of the physics. The work described here is an example of this. By adding just the most basic physics of pickup ions to our model, we have brought it into better agreement with spacecraft observations. In extending our model to 100 AU, we expect that in order to reproduce temperature vs. distance and other observations in the more distant outer heliosphere, we will find it helpful to add more such modifications. In particular, our current use of a polytropic index to implicitly represent thermal heat conduction based on work by *Totten et al.* [1996] is certainly not valid far beyond 1 AU; we plan to rectify this by introducing some explicit form of heat or energy transport, such as the collisionless electron heat conduction of *Hollweg* [1976], or the Alfvén wave energy flux of *Usmanov et al.* [2000]. Also since energetic particles (pickup ions) account for most of the thermal pressure in the distant heliosphere, we may eventually want to consider the effect of turbulence energy resulting from the effect of the pickup process on the magnetic field, as described by *Isenberg et al.* [2010].

[36] Large-scale models, such as HHMS-PI, generally cannot include microscale physics in detail, even when it is well known. Consequently, the success of a large-scale model often depends on finding useful (or even correct) empirical relationships that capture the emergent macroscale consequences of the microphysics. The interface module in HHMS-PI takes this approach. It maps source surface model outputs at $5R_S$ into MHD boundary conditions at $21.5R_S$ using a set of empirical formulas (equations (1)–(8)) to produce the background solar wind in HHMS-PI. Comparison of equations (1)–(8) here with the corresponding equations of *Detman et al.* [2006] show that the interface module has evolved. In fact, at this stage of development, the interface model continues to evolve, as our understanding of the corona improves. In the near future we hope to explore other important parts of the model for further improvement, such as our current 5° × 5° angular grid resolution, our oversimplified background neutral hydrogen distribution, or our diffusive, modified two-step Lax-Wendroff numerical scheme [*Han et al.*, 1988]. In spite of these self-deprecating statements, we have prominently displayed skill scores, and correlation coefficients, on all

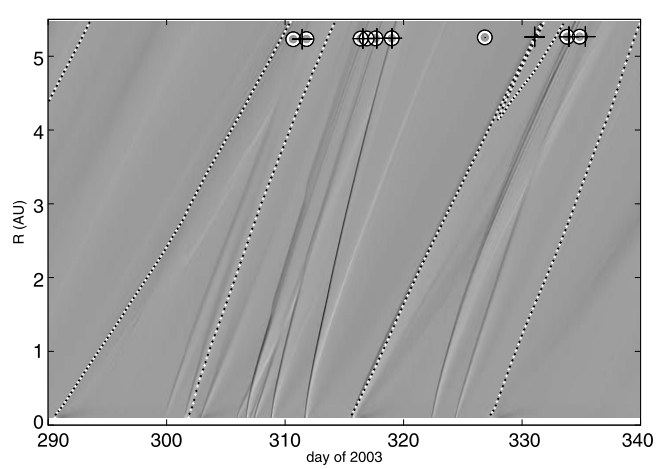

Figure 4. Sun-Ulysses r-t plot of shock index. Circles mark observed shock arrivals; plus signs mark simulated shock arrivals. Dotted lines mark magnetic sector boundaries.

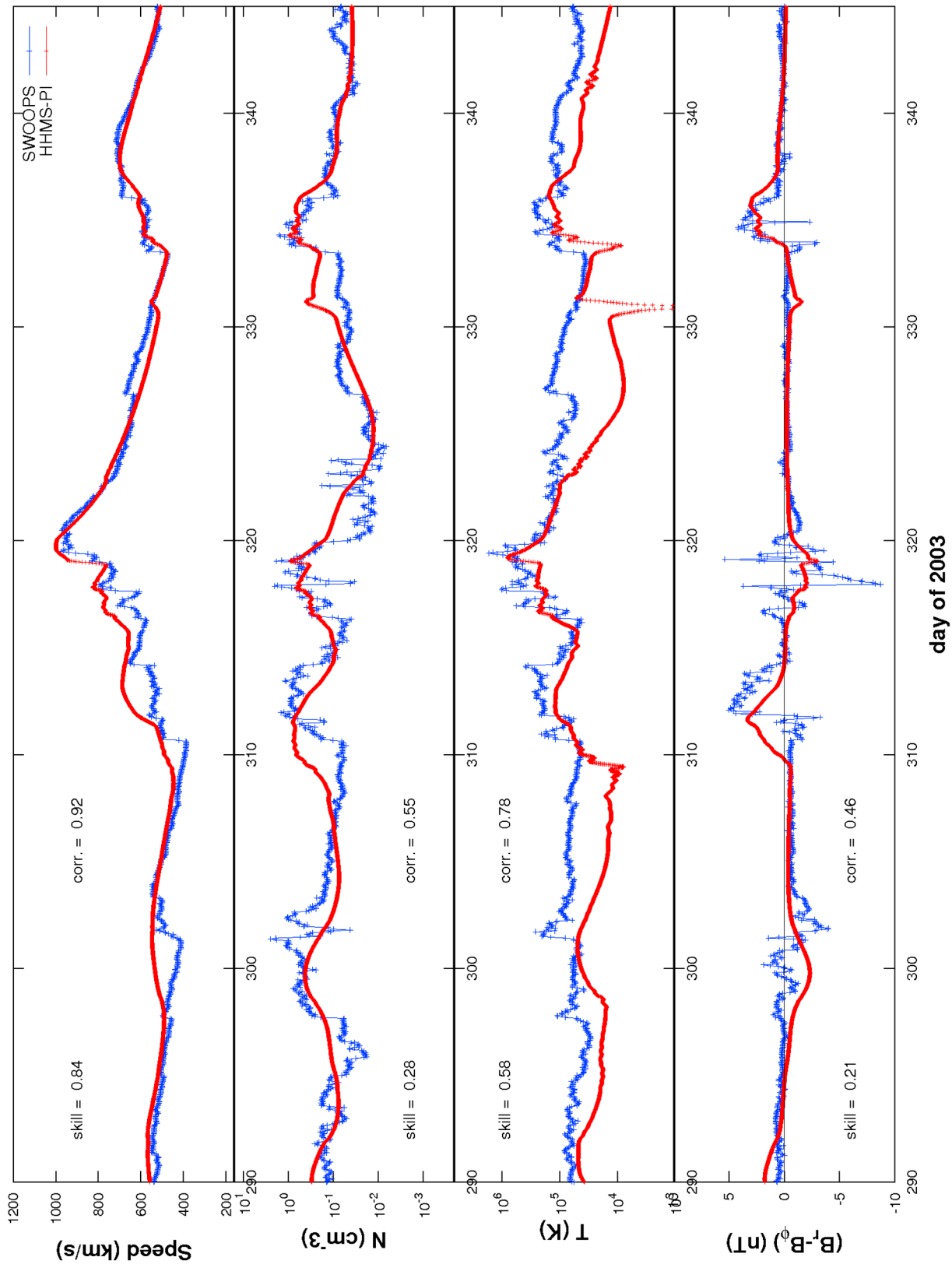

Figure 5. Comparison of HHMS-PI simulated time series at Ulysses with Ulysses solar wind observations for the Halloween 2003 study interval. Blue is Ulysses SWOOPS data. Red is HHMS-PI.

Table 4. Shock Arrival Delays at Ulysses Due to Pickup Protons[a]

FF	DOYSUN	OBSULY	$DNH_0 = 0.1$	$DNH_0 = 0$	DIFF (days)
514	301.460	311.801	312.632	311.877	0.755
517	306.718	316.884	317.876	317.000	0.876
520	308.822	317.641	318.194	317.491	0.703
520.2	311.664	319.000	319.167	318.600	0.567
521	315.566	326.851	327.004	326.105	0.899
524	322.324	333.810	335.145	334.534	0.611

[a]FF, event sequence number; DOYSUN, FF solar event day of 2003 with fraction; OBSULY, observed shock arrival at Ulysses day of 2003 with fraction; DNH0.1, simulated Ulysses shock arrival day of 2003 with fraction for the case of neutral hydrogen density at $\infty = 0.1$ cm^3; DNH0.0, simulated Ulysses shock arrival day of 2003 with fraction for the case of neutral hydrogen density equal to zero; DIFF, DIFF = DNH0.1 − DNH0.0.

panels in both Figures 3 and 5. And, we hasten to add, that such numbers are sensitive to both the interval over which they are calculated, and to the time resolution of the verification data. It has been said, that publishing such numbers can be self-limiting, providing an easy target for critics. Nevertheless, in the interest of science, openness and transparency, we pursue full disclosure.

5. Conclusions

[37] The general agreement of HHMS-PI simulation results with ACE observations shown in Figure 3, and with Ulysses observations shown in Figure 5, demonstrate that HHMS-PI is a suitable foundation for extending our benchmarking process for tracking shocks out to Cassini and beyond. Our results also clearly demonstrate the impact of including pickup proton effects in our model. This important success highlights the fact that our full 3-D model offers extensibility to include a range of physical phenomena that can even further strengthen our model. We are very encouraged by the level of agreement shown here, and we plan to continue addressing the bountiful avenues of model applications and improvements that we have identified.

Appendix A

[38] HHMS-PI computational equations (heliocentric spherical coordinates):

$$\frac{\partial \mathbf{U}}{\partial t} + \frac{\partial \mathbf{F}}{\partial r} + \frac{1}{r\sin\theta}\frac{\partial \mathbf{G}}{\partial \theta} + \frac{1}{r\sin\theta}\frac{\partial \mathbf{H}}{\partial \phi} = \mathbf{S},$$

where

$$\mathbf{U} = \begin{Bmatrix} r^2\rho_S \\ r^2\rho U_r \\ r^2\rho U_\theta \\ r^2\rho U_\phi \\ r^2 B_r \\ rB_\theta \\ rB_\phi \\ r^2\rho\left[\frac{U^2}{2} + \frac{P}{(\gamma-1)\rho} + \frac{A^2}{2}\right] \\ r^2\rho_I \\ r^2 P_I^{3/5} \end{Bmatrix},$$

$$\mathbf{F} = \begin{Bmatrix} r^2\rho_S U_r \\ r^2\rho\left(U_r^2 + \frac{P}{\rho} + \frac{A^2}{2} - A_r^2\right) \\ r^2\rho(U_rU_\theta - A_rA_\theta) \\ r^2\rho\left(U_rU_\phi - A_rA_\phi\right) \\ 0 \\ r(U_rB_\theta - B_rU_\theta) \\ r\left(U_rB_\phi - B_rV_\phi\right) \\ r^2\rho\Big[U_r\left(\frac{U^2}{2} + \frac{\gamma P_S}{(\gamma-1)\rho} + \frac{5}{2}\frac{P_I}{\rho}\right) \\ \quad + A_\theta(U_rA_\theta - A_rU_\theta) + A_\phi\left(U_rA_\phi - A_rV_\phi\right) - wA_rA_\phi\Big] \\ r^2\rho_I U_r \\ r^2 P_I^{3/5} U_r \end{Bmatrix},$$

$$\mathbf{G} = \begin{Bmatrix} r^2\sin\theta\rho_S U_\theta \\ r^2\rho\sin\theta(U_rU_\theta - A_rA_\theta) \\ r^2\rho\sin\theta\left(U_\theta^2 + \frac{P}{\rho} + \frac{A^2}{2} - A_\theta^2\right) \\ r^2\rho\sin\theta\left(U_\phi U_\theta - A_\theta A_\phi\right) \\ r^2\sin\theta(U_\theta B_r - B_\theta U_r) \\ 0 \\ r\sin\theta\left(U_\theta B_\phi - B_\theta V_\phi\right) \\ r^2\rho\sin\theta\Big[U_\theta\left(\frac{U^2}{2} + \frac{\gamma P_S}{(\gamma-1)\rho} + \frac{5}{2}\frac{P_I}{\rho}\right) \\ \quad - A_r(U_rA_\theta - A_rU_\theta) + A_\phi\left(U_\theta A_\phi - A_\theta V_\phi\right) - wA_\theta A_\phi\Big] \\ r^2\sin\theta\rho_I U_\theta \\ r^2\sin\theta P_I^{3/5} U_\theta \end{Bmatrix},$$

$$\mathbf{H} = \begin{Bmatrix} r^2\rho_S V_\phi \\ r^2\rho\left(U_rV_\phi - A_rA_\phi\right) \\ r^2\rho\left(U_\theta V_\phi - A_\theta A_\phi\right) \\ r^2\rho\left(U_\phi V_\phi + \frac{P}{\rho} + \frac{A^2}{2} - A_\phi^2\right) \\ r^2\left(V_\phi B_r - B_\phi U_r\right) \\ r\left(V_\phi B_\theta - B_\phi U_\theta\right) \\ 0 \\ r^2\rho\Big[V_\phi\left(\frac{U^2}{2} + \frac{\gamma P_S}{(\gamma-1)\rho} + \frac{5P_I}{2\rho}\right) + A_r\left(V_\phi A_r - U_rA_\phi\right) \\ \quad - A_\theta\left(U_\theta A_\phi - A_\theta V_\phi\right) + w\left(\frac{P}{\rho} + \frac{A^2}{2} - A_\phi^2\right)\Big] \\ r^2\rho_I V_\phi \\ r^2 P_I^{3/5} V_\phi \end{Bmatrix},$$

$$\mathbf{S} = \begin{Bmatrix} -r^2 q_{ex} \\ r\rho\left[\left(U_\theta^2 + U_\phi^2\right) + 2\frac{P}{\rho} + A_r^2\right] - \rho GM_S - r^2U_rq_{ex} \\ r\rho\left[-(U_rU_\theta - A_rA_\theta) - \cot\theta\left(U_\phi^2 + \frac{P}{\rho} + \frac{A^2}{2} - A_\phi^2\right)\right] \\ \quad - r^2U_\theta q_{ex} \\ r\rho\left[-\left(U_rU_\phi - A_rA_\phi\right) - \cot\theta\left(U_\theta U_\phi - A_\theta A_\phi\right)\right] \\ \quad - r^2U_\phi q_{ex} \\ 0 \\ 0 \\ \cot\theta\left(U_\theta B_\phi - B_\theta V_\phi\right) \\ -\rho U_r GM_S \ - r^2 q_{ex}\left[\frac{U^2}{2} + \frac{\gamma P_S}{(\gamma-1)\rho_S}\right] \\ +r^2\left(q_{ex} + q_{ph}\right) \\ \frac{+r^2U^2\left(q_{ex}+q_{ph}\right)}{5P_I^{2/5}} \end{Bmatrix},$$

where $\rho = \rho_S + \rho_I$, $P = P_S + P_I$, $P_S = 2\rho_S RT_S$, $P_I = \rho_I RT_I$, $U^2 = U_r^2 + U_\theta^2 + U_\phi^2$, $A^2 = A_r^2 + A_\theta^2 + A_\phi^2$, $A_{r,\theta,\phi}^2 = B_{r,\theta,\phi}^2/(\rho\mu_0)$. Here U denotes velocity in the inertial frame, V denotes

velocity in the solar corotating frame, $\mathbf{U} = \mathbf{V} + \mathbf{w}$, where $\mathbf{w} = \Omega \times \mathbf{r} = \Omega r \sin\theta\hat{\phi}$, and Ω is the solar rotation rate.

[39] Also, ρ_S and P_S are solar wind density and pressure; ρ_I and P_I are pickup ion density and pressure. The ratio of specific heats for pickup ions is taken to be 5/3; the polytropic index for the solar wind is $\gamma = 1.5$. For our steady state model, used only to initialize our time-dependent model, and for this initial development of the time-dependent model, we use the spherically symmetric and stationary (with respect to the Sun) neutral hydrogen distribution given by *Wang et al.* [2000]: $N_H = N_\infty e^{-\lambda/r}$, where $N_\infty = 0.1$ cm^{-3}, and $\lambda = 4$ AU. Following *Whang* [1998] and *Usmanov and Goldstein* [2006], the production rates for interstellar pickup ions are given by: $q_{ex} = \sigma m_p N_S N_H\,|\mathbf{U}|$, $q_{ph} = \nu m_p N_H \left(\frac{r_0^2}{r^2}\right)$, with $\sigma = 2 \times 10^{-15}$ cm^2, and $\nu = 9 \times 10^{-8}\ s^{-1}$, as in work by *Usmanov and Goldstein* [2006]. We plan to introduce more realistic models for N_H in future work. Also, for some runs in the current work, we set $N_H = 0$ to determine the specific affects due to pickup protons.

[40] **Acknowledgments.** We thank the NOAA Space Weather Prediction Center for generating and maintaining the archives of WSA source surface maps and making them available. We thank the ACE and Ulysses teams and the NSSDC for the IMF, plasma, and plasma wave data and trajectory information. We thank A. Usmanov for invaluable help in deriving the computational equations in Appendix A. This work was supported in part by NASA grant NNX08AE40G with Carmel Research Center and in part by Carmel Research Center. T. R. Detman thanks the Ubuntu, Octave, OpenOffice.org, and LaTeX open source project communities.

[41] Philippa Browning thanks Melvyn Goldstein and another reviewer for their assistance in evaluating this paper.

References

Arge, C. N., and V. Pizzo (2000), Improvement in the prediction of solar wind conditions using near-real time solar magnetic field updates, *J. Geophys. Res.*, *105*, 10,465–10,479.

Burlaga, L., N. Ness, M. Acuna, R. P. Lepping, J. Connery, and J. Richardson (2008), Magnetic fields at the solar wind termination shock, *Nature*, *454*, 75–77, doi:10.1038/nature 07029.

de Koning, C. A., et al. (2005), An unusually fast interplanetary coronal mass ejection observed by Ulysses at 5 AU on 15 November 2003, *J. Geophys. Res.*, *110*, A01102, doi:10.1029/2004JA010645.

Detman, T. R., and D. Vassiliadis (1997), Review of techniques for magnetic storm forecasting, in *Magnetic Storms*, *Geophys. Monogr. Ser.*, vol. 98, edited by Y. K. Bruce et al., pp. 253–266, AGU, Washington, D. C.

Detman, T., Z. Smith, M. Dryer, C. Fry, C. Arge, and V. Pizzo (2006), A hybrid heliospheric modeling system: I. Background solar wind, *J. Geophys. Res.*, *111*, A07102, doi:10.1029/2005JA011430.

Dryer, M., Z. Smith, C. Fry, W. Sun, C. Deehr, and S.-I. Akasofu (2004), Real-time predictions of interplanetary shock arrivals at L1 during the Halloween 2003 epoch, *Space Weather*, *2*, S09001, doi:10.1029/2004SW000087.

Fry, C. D., W. Sun, C. Deehr, M. Dryer, Z. Smith, S.-I. Akasofu, M. Tokumaru, and M. Kojima (2001), Improvements to the HAF solar wind model for space weather predictions, *J. Geophys. Res.*, *106*, 20,985–21,001.

Fry, C. D., M. Dryer, Z. Smith, W. Sun, C. S. Deehr, and S.-I. Akasofu (2003), Forecasting solar wind structures and shock arrival times using an ensemble of models, *J. Geophys. Res.*, *108*(A2), 1070, doi:10.1029/2002JA009474.

Han, S. M., S. Wu, and M. Dryer (1988), A three-dimensional, time-dependent, numerical modeling of super-sonic, super-Alfvenic MHD flow, *Comput. Fluids*, *16*, 81–103.

Hollweg, J. V. (1976), Collisionless electron heat conduction in the solar wind, *J. Geophys. Res.*, *81*, 1649–1658.

Intriligator, D., W. Sun, M. Dryer, C. Fry, C. Deehr, and J. Intriligator (2005a), From the Sun to the outer heliosphere: Modeling and analyses of the interplanetary propagation of the October/November (Halloween) 2003 solar events, *J. Geophys. Res.*, *110*, A09S10, doi:10.1029/2004JA010939.

Intriligator, D. S., T. Detman, M. Dryer, C. G. Fry, W. Sun, C. Deehr, and J. Intriligator (2005b), Initial comparisons between a 3D MHD approach and the HAFv2 kinematic model: The Halloween 2003 events from the Sun to 6 AU, in *The Physics of Collisionless Shocks: 4th Annual IGPP International Astrophysics Conference: Palm Springs, California, 26 February–3 March, 2005*, edited by G. Li, pp. 304–309, Am. Inst. of Phys., Melville, N. Y.

Intriligator, D. S., T. Detman, W. Sun, C. Fry, M. Dryer, C. Deehr, Z. Smith, and J. Intriligator (2005c), Asymmetries in the solar wind from the Sun to 10 AU: Comparison between a 3D MHD approach and the 3D HAFv2 kinematic model, in *Connecting Sun and Heliosphere: Proceedings of Solar Wind 11/SOHO 16: 12–17 June 2005, Whistler, Canada*, pp. 343–346, Eur. Space Agency, Noordwijk, Netherlands.

Intriligator, D., W. Sun, T. Detman, M. Dryer, C. G. Fry, C. Deehr, and J. Intriligator (2006), Solar variability effects in the outer heliosphere and heliosheath, in *Physics of the Inner Heliosheath: Voyager Observations, Theory, and Future Prospects: 5th Annual IGPP International Astrophysics Conference*, edited by J. Heerikhuisen et al., pp. 64–70, Am. Inst. of Phys., Melville, N. Y.

Intriligator, D., A. Rees, T. Horbury, W. Sun, T. Detman, M. Dryer, C. Deehr, and J. Intriligator (2007), 3D modeling and turbulence: From the Sun to Voyager 1, in *Turbulence and Nonlinear Processes in Astrophysical Plasmas: 6th Annual International Astrophysics Conference, Oahu, Hawaii, 16–22 March 2007*, edited by D. Shaikh and G. P. Zank, pp. 167–174, Am. Inst. of Phys., Melville, N. Y.

Intriligator, D., A. Rees, T. Horbury, W. Webber, C. Deehr, T. Detman, M. Dryer, and J. Intriligator (2008), Three-dimensional simulations of shock propagation in the heliosphere and beyond, in *Particle Acceleration and Transport in the Heliosphere and Beyond: 7th Annual International Astrophysics Conference, Kauai, Hawaii, 7–13 March 2008*, edited by G. Li et al., pp. 375–383, Am. Inst. of Phys., Melville, N. Y.

Intriligator, D. S., J. Intriligator, W. D. Miller, W. R. Webber, and R. B. Decker (2010a), Higher-energy plasma ions found near the termination shock: Analyses of Voyager 2 data in the heliosheath and in the outer heliosphere, *J. Geophys. Res.*, *115*, A07107, doi:10.1029/2009JA014967.

Intriligator, D., J. Intriligator, W. D. Miller, W. R. Webber, R. B. Decker, W. Sun, T. Detman, M. Dryer, and C. Deehr (2010b), Voyager 2 high energy ions near the outward moving termination shock, in *Pickup Ions Throughout the Heliosphere and Beyond: Proceedings of the 9th Annual International Astrophysics Conference*, edited by J. le Roux et al., pp. 148–157, Am. Inst. of Phys., Melville, N. Y.

Isenberg, P. A., C. W. Smith, W. H. Matthaeus, and J. D. Richardson (2010), Turbulent heating of the distant solar wind by interstellar pickup protons in a decelerating flow, *Astrophys. J.*, *719*, 716–721.

MacNiece, P. (2009), Validation of community models: Identifying events in space weather model timelines, *Space Weather*, *7*, S06004, doi:10.1029/2009SW000463.

McKenna-Lawlor, S., M. Dryer, M. Kartalev, Z. Smith, C. Fry, W. Sun, C. Deehr, K. Kecskemety, and K. Kudela (2006), Near real-time predictions of the arrival at the Earth of flare-generated shocks during solar cycle 23, *J. Geophys. Res.*, *111*, A11103, doi:10.1029/2005JA011162.

Richardson, J., J. Kasper, C. Wang, J. Belcher, and A. Lazarus (2008), Cool heliosheath plasma and deceleration of the upstream solar wind at the termination shock, *Nature*, *454*, 63–65, doi:10:1038/nature07024.

Smith, Z. K., R. Steenburgh, C. D. Fry, and M. Dryer (2009a), Predictions of interplanetary shock arrivals at Earth: Dependence of forecast outcome on the input parameters, *Space Weather*, *7*, S12005, doi:10.1029/2009SW000500.

Smith, Z. K., M. Dryer, S. McKenna-Lawlor, C. Fry, C. Deehr, and W. Sun (2009b), Operational validation of HAF's predictions of interplanetary shock arrivals at Earth: Declining phase of solar cycle 23, *J. Geophys. Res.*, *114*, A05106, doi:10.1029/2008JA013836.

Totten, T. L., J. Freeman, and S. Arya (1996), Application of the empirically derived polytropic index for the solar wind to models of solar wind propagation, *J. Geophys. Res.*, *101*, 15,629–15,635.

Usmanov, A., and M. Goldstein (2006), A three-dimensional MHD solar wind model with pickup protons, *J. Geophys. Res.*, *111*, A07101, doi:10.1029/2005JA011533.

Usmanov, A. V., M. L. Goldstein, B. P. Besser, and J. M. Fritzer (2000), A global MHD solar wind model with WKB Alfvén waves: Comparison with Ulysses data, *J. Geophys. Res.*, *105*, 12,765–12,695.

Veselovsky, I., et al. (2004), Solar and heliospheric phenomena in October–November 2003: Causes and effects, *Cosmic Res., Engl. Transl.*, *42*(5), 435–488.

Wang, C., J. Richardson, and J. Gosling (2000), A numerical study of the evolution of the solar wind from Ulysses to Voyager 2, *J. Geophys. Res.*, *105*, 2337–2344.

Wang, Y. M., and N. Sheeley (1988), The solar origin of long-term variations of the interplanetary magnetic field strength, *J. Geophys. Res.*, *93*, 11,227–11,236.
Wang, Y. M., and N. Sheeley (1990), Solar wind speed and coronal flux-tube expansion, *Astrophys. J.*, *355*, 726–732.
Wang, Y.-M., S. H. Hawley, and N. R. Sheeley Jr. (1996), The magnetic nature of coronal holes, *Science*, *271*, 464–469.
Wang, Y. M., N. Sheeley, J. Phillips, and B. Goldstein (1997), Solar wind stream interactions and wind speed-expansion factor relationship, *Astrophys. J.*, *488*, L51–L54.
Whang, Y. (1998), Solar wind in the distant heliosphere, *J. Geophys. Res.*, *103*, 17,419–17,428.
Zhao, X., and J. T. Hoeksema (1993), Unique determination of model coronal magnetic fields using photospheric observations, *Sol. Phys.*, *143*, 41–48.
Zhao, X., and J. T. Hoeksema (1994), A coronal magnetic field model with horizontal volume and sheet currents, *Sol. Phys.*, *151*, 91–105.
Zhao, X., and J. T. Hoeksema (1995), Prediction of the interplanetary magnetic field strength, *J. Geophys. Res.*, *100*, 19–33.

C. S. Deehr, Geophysical Institute, University of Alaska Fairbanks, Fairbanks, AK 99775, USA. (cdeehr@gi.alaska.edu)
T. R. Detman, M. Dryer, D. S. Intriligator, and W. Sun, Carmel Research Center, PO Box 1732, Santa Monica, CA 90406, USA. (tmdetman@earthlink.net; murraydryer@msn.com; devriei@aol.com; wsun_1939@yahoo.com)
J. Intriligator, Bangor University, Bangor LL57 2AS, UK. (jamesi@post.harvard.edu)